Multiphoton correlations between quantum images

Serge Massar,[1] Fabrice Devaux,[2] and Eric Lantz[2]
[1]*Laboratoire d'Information Quantique CP224, Université libre de Bruxelles, Avenue F. D. Roosevelt 50, B-1050 Bruxelles, Belgium*
[2]*Institut FEMTO-ST, Département d'Optique, UMR 6174, Centre National de la Recherche Scientifique, Université de Franche-Comté, 15 B rue des Montboucons, 25030 Besançon, France*

(Received 4 November 2022; revised 19 May 2023; accepted 27 June 2023; published 13 July 2023)

Experimental demonstrations of entangled quantum images produced through parametric down conversion have so far been confined to studying two-photon correlations. Here we show that multiphoton correlations between quantum images are accessible experimentally and exhibit many new features including being sensitive to the phase of the biphoton wave function. As a concrete example, we consider a modification of existing quantum imaging experiments in which the charge-coupled device cameras are moved out of focus, provide detailed analytical predictions for the resulting four-photon interferences, and support these by numerical simulations. The proposed experiment can also be interpreted as entanglement swapping: Bob's photons are initially unentangled, but the joint detection of Alice's photons projects Bob's photons onto an entangled state. The general approach proposed here can be extended to other quantum optics experiments involving high-dimensional entanglement.

DOI: 10.1103/PhysRevA.108.013705

I. INTRODUCTION

Since the seminal works of Freedman and Clauser [1] and Aspect and Dalibard [2], entangled photons have been one of the workhorses of quantum information sciences. Nowadays high-dimensional entangled photon pairs can be routinely produced in the laboratory, using different degrees of freedom such as angular momentum [3,4], time-energy [5–8], position-momentum [9–12], path entanglement (using integrated optics) [13], or multiple degrees of freedom simultaneously [14]. The number of modes that can be entangled can reach hundreds, or even thousands (see, e.g., [4,8,10–12]). These experiments have focused on the correlations between two entangled photons. Here we show that if one extends them to the study of multiphoton correlations, then novel phenomenology and interference patterns emerge. These new features are experimentally accessible with current technology, as they already appear in four-photon correlations. In the same way that the quantum teleportation experiment of Bouwmeester *et al.* [15] revolutionized quantum optics, we expect the present proposal to considerably broaden the scope and interest of high-dimensional photonic entanglement.

An important inspiration for the present paper is boson sampling [16] (see the experimental realizations of [17–21]). On the one hand boson sampling provides the theoretical framework for describing multiphoton correlations. On the other hand the computational complexity arguments of [16] show that as the number of modes and the number of photons increase, the correlation pattern become exceedingly complex and impossible to simulate efficiently on a classical computer. But for a moderate number of photons (say 4 or 6), while this complexity already shows up, it should be possible to fully investigate the system experimentally. The present paper is most closely related to the extension of boson sampling to Gaussian bipartite states [22,23], and to the low optical depth boson sampling of [24].

For definiteness we illustrate our approach in the case of spatially entangled photons, as realized in [10,11], and schematized in Fig. 1. A spatially extended, pulsed, pump laser illuminates a thin nonlinear crystal in which photon pairs are produced by spontaneous parametric down conversion (SPDC) using type-II phase matching. The signal and idler photons are not collinear and are imaged separately on Alice's and Bob's cameras. Single-photon resolution on each pixel of the camera is achieved by using electron multiplying charge-coupled devices (CCDs). Such quantum imaging experiments were introduced theoretically in [25]. Using CCD cameras, they have been applied to demonstrations of the Einstein-Podolsky-Rosen paradox [11,26], ghost imaging [27], quantum adaptive optics [28], quantum holography [12], sub-shot-noise imaging [29,30], and quantum imaging with undetected photons [31] (see [32] for a review). Note that additional optical elements, such as a spatial light modulator (SLM), or a diffuser [28,33], can be inserted between the source and the CCD if desired. Ghost imaging with entanglement-swapped photons was reported in [34] demonstrating the feasibility of multiphoton quantum imaging experiments.

Here we consider multiphoton correlations on the image planes. If the produced photons are indistinguishable (except for the position-momentum degree of freedom), then we do not know which photon detected on Alice's camera is the partner of which photon detected on Bob's camera. The probability for a specific detection event is obtained by summing all the possible pairings of signal and idler photons, as illustrated in Fig. 1 in the case of four-photon correlations.

II. MULTIPHOTON CORRELATIONS IN QUANTUM IMAGES

We treat the pump beam classically which implies that the quantum state of the signal and idler photons is Gaussian and

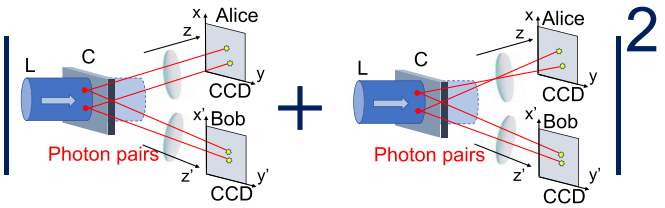

FIG. 1. Schematic of the proposed setup and interferences between four-photon correlations. A spatially extended, pulsed, pump laser (L) generates photon pairs in a nonlinear crystal (C) through spontaneous parametric down conversion. The signal and idler photons (red lines) are imaged onto Alice's and Bob's CCD cameras. If two photons are detected on Alice's camera and two photons are detected on Bob's camera, then we don't know which photon is the partner of which photons. The amplitudes for the two processes interfere, and must be summed when computing the probability of this event [see Eq. (4)]. This is indicated schematically in the figure by the "+" sign between the two amplitudes which must be taken before squaring. x, y, z and x', y', z' are the coordinates used in the main text. The lens in the image indicates schematically that an imaging system is used, specifically either a $2f$ or $4f$ optical system, slightly defocused as measured by z and z'.

can be written as

$$|\Psi\rangle = N \exp\left(\iint d\mathbf{x} d\mathbf{x}' \Phi(\mathbf{x}, \mathbf{x}') a^\dagger_{\mathbf{x}} a^\dagger_{\mathbf{x}'}\right)|0\rangle, \tag{1}$$

where $\Phi(\mathbf{x}, \mathbf{x}')$ is the biphoton wave function with $\mathbf{x} = (x, y)$ and $\mathbf{x}' = (x', y')$ the positions on Alice's and Bob's image planes [we denote throughout Alice's (Bob's) variables with unprimed (primed) letters], $a^\dagger_{\mathbf{x}}$ and $a^\dagger_{\mathbf{x}'}$ are creation operators for photons at $\mathbf{x}$ and $\mathbf{x}'$, $|0\rangle$ is the vacuum state, and N is a normalization factor.

The probability of detecting n photons on Alice's camera at positions $\mathbf{X}_{(n)} = \mathbf{x}_1, \cdots, \mathbf{x}_n$ and n photons on Bob's camera at positions $\mathbf{X}'_{(n)} = \mathbf{x}'_1, \cdots, \mathbf{x}'_n$ is given by [22,23]

$$\begin{aligned} P^{(2n)}(\mathbf{X}_{(n)}; \mathbf{X}'_{(n)}) &= |\langle 0| a_{\mathbf{x}_1} \cdots a_{\mathbf{x}_n} a_{\mathbf{x}'_1} \cdots a_{\mathbf{x}'_n} |\Psi\rangle|^2 \\ &= |N|^2 |\mathrm{Perm}(\Phi_{\mathbf{x}_1, \cdots, \mathbf{x}_n; \mathbf{x}'_1, \cdots, \mathbf{x}'_n})|^2 \end{aligned} \tag{2}$$

where $\Phi_{\mathbf{x}_1, \cdots, \mathbf{x}_n; \mathbf{x}'_1, \cdots, \mathbf{x}'_n}$ is the $n \times n$ matrix whose (i, j)th entry is given by the biphoton wave function at positions $(\mathbf{x}_i, \mathbf{x}'_j)$, i.e., by $\Phi(\mathbf{x}_i, \mathbf{x}'_j)$, and Perm is the permanent of the matrix.

In order to simplify expressions, we make the following approximations. First, in order to get the response of the camera we need to integrate Eq. (2) over the area of each pixel. We assume that Φ varies little over the area of a pixel and therefore omit this integration. Second we assume that the mean number of photons is much smaller than the number of pixels, and consequently the probability of two photons reaching the same pixel is small, and we do not consider these events. Third we assume that losses are negligible.

Thus the probability of detecting a single pair at positions $(\mathbf{x}; \mathbf{x}')$ is given by

$$P^{(2)}(\mathbf{x}; \mathbf{x}') = |N|^2 |\Phi(\mathbf{x}, \mathbf{x}')|^2, \tag{3}$$

and depends only on the norm of the biphoton wave function. But if two pairs are detected at $(\mathbf{x}_1, \mathbf{x}_2)$ and $(\mathbf{x}'_1, \mathbf{x}'_2)$, then the corresponding probability is given by

$$\begin{aligned} P^{(4)}(\mathbf{x}_1, \mathbf{x}_2; \mathbf{x}'_1, \mathbf{x}'_2) = |N|^2 |&\Phi(\mathbf{x}_1, \mathbf{x}'_1)\Phi(\mathbf{x}_2, \mathbf{x}'_2) \\ &+ \Phi(\mathbf{x}_1, \mathbf{x}'_2)\Phi(\mathbf{x}_2, \mathbf{x}'_1)|^2. \end{aligned} \tag{4}$$

A new interference effect arises because we do not know whether the photon detected at $\mathbf{x}_1$ is the partner of the photon detected at $\mathbf{x}'_1$ or at $\mathbf{x}'_2$, and we must sum the amplitudes for these two processes as illustrated in Fig. 1. Therefore Eq. (4) is sensitive to the phase of the biphoton wave function.

III. DEFOCUSING THE QUANTUM IMAGES

For the purpose of analytical predictions, we assume that the biphoton wave function is Gaussian, which is a widely used and well-justified approximation [35–37]. At the surface of the nonlinear crystal (i.e., in the near field) the biphoton wave function is thus given by

$$\Phi(\mathbf{x}, \mathbf{x}') \propto \exp\left(-\frac{1}{4w_0^2}|\mathbf{x} + \mathbf{x}'|^2 - \frac{b^2}{4}|\mathbf{x} - \mathbf{x}'|^2\right). \tag{5}$$

For simplicity of notation we omit, here and in the following expressions, the constant that multiplies the exponentials in Φ, and denote this by the symbol $\propto$. In Eq. (5), w_0 is the width of the pump beam, while b takes into account that the phase-matching conditions are only partially enforced due to the finite thickness of the nonlinear crystal. The photon pairs are produced approximately in the same location, up to an uncertainty $1/b$. The Schmidt number of this biphoton wave function is $K = \frac{1}{4}(bw_0 + \frac{1}{bw_0})^2$[35]. We are interested in the situation where $w_0 \gg 1/b$, corresponding to a large area of illumination of the crystal and a high Schmidt number. Experimentally the total number of spatial modes in entangled images of order 2000 is reported [10], although direct measurements of the Schmidt number have yielded a lower value of order 200 [11].

The Fourier transform of Eq. (5) gives the biphoton wave function in the far field

$$\tilde{\Phi}(\mathbf{p}, \mathbf{p}') \propto \exp\left(-\frac{w_0^2}{4}|\mathbf{p} + \mathbf{p}'|^2 - \frac{1}{4b^2}|\mathbf{p} - \mathbf{p}'|^2\right) \tag{6}$$

where $\mathbf{p}$ and $\mathbf{p}'$ are the transverse momenta of Alice's and Bob's photons.

For interesting interferences to arise in the four-photon coincidences Eq. (4) we need a complex, oscillating biphoton wave function. This is not the case for the near- and far-field biphoton wave functions Eqs. (5) and (6) which are real and positive. But in [37] it was shown that as the photons propagate, the entanglement between Alice's and Bob's photons becomes encoded in the phase of the biphoton wave function. This situation is a readily accessible regime experimentally: One simply needs to move the cameras out of focus. Note that because of the symmetry between Eqs. (5) and (6) one could either defocus the near-field image or the far-field image. Below we consider the case of defocusing the near-field image.

If Alice's and Bob's photons travel a distance z and z' from the crystal surface, then in the paraxial approximation, the

biphoton wave function in momentum space is given by

$$\tilde{\Phi}(\mathbf{p},\mathbf{p}';z,z') \propto \exp\left(-\frac{w_0^2}{4}|\mathbf{p}+\mathbf{p}'|^2 - \frac{1}{4b^2}|\mathbf{p}-\mathbf{p}'|^2 - i\frac{z}{2k}|\mathbf{p}|^2 - i\frac{z'}{2k}|\mathbf{p}'|^2\right) \tag{7}$$

where k is the longitudinal momenta of the idler and signal photons (assumed equal). In order to simplify the expression for the Fourier transform of Eq. (7), we take the limit $w_0 \to \infty$ in the resulting expression, whereupon $\Phi(\mathbf{x},\mathbf{x}';z,z')$ only depends on $\mathbf{x}-\mathbf{x}'$, i.e., we are in the translation invariant limit. We then have

$$\Phi(\mathbf{x},\mathbf{x}';z,z') \propto \exp\left(-\frac{\alpha-i\beta}{4}|\mathbf{x}-\mathbf{x}'|^2\right) \tag{8}$$

where $\alpha = \frac{b^2}{1+Z^2}$ and $\beta = \frac{b^2 Z}{1+Z^2}$ are real and positive with $Z = \frac{b^2(z+z')}{2k}$. The uncertainty in the joint positions is of size $1/\sqrt{\alpha}$, and increases when the defocusing (i.e., z and z') increases. The defocusing is important when $Z \gg 1$, whereupon $\beta \gg \alpha$, and the biphoton wave function exhibits many oscillations within a defocusing spot.

Going back to Fig. 1, Eqs. (5), (6), and (8) correspond to the biphoton wave function on the camera planes when imaging the near field (the crystal surface), the far field, and the defocused near field, respectively. The coordinates (x,y) and (x',y') in Fig. 1 correspond to $\mathbf{x}$ and $\mathbf{x}'$ in the case of Eqs. (5) and (8) and to $\mathbf{p}$ and $\mathbf{p}'$ in the case of Eq. (6), while the z and z' coordinates correspond to the degree of defocusing.

In order to obtain predictions for the four-photon correlations, we insert Eq. (8) into Eq. (4). One finds that the four-photon correlation probability takes the simple form

$$P^{(4)}(\mathbf{X};\mathbf{X}';z,z') \propto \exp\left(-\frac{\alpha}{4}D\right)\left(\cosh\left(\frac{\alpha}{2}S\right)+\cos\left(\frac{\beta}{2}S\right)\right) \tag{9}$$

where $D(\mathbf{X};\mathbf{X}') = |\mathbf{x_1} - \mathbf{x_1'}|^2 + |\mathbf{x_1}-\mathbf{x_2'}|^2 + |\mathbf{x_2}-\mathbf{x_1'}|^2 + |\mathbf{x_2}-\mathbf{x_2'}|^2$ and $S(\mathbf{X};\mathbf{X}') = (\mathbf{x_1}-\mathbf{x_2}).(\mathbf{x_1'}-\mathbf{x_2'})$. When the defocusing is significant ($\beta \gg \alpha$) then the four-photon coincidence probabilities have strong oscillations given by the term $\cos(\frac{\beta}{2}S)$. In Appendix A we show that the oscillating term in Eq. (9) [the term in $\cos(\frac{\beta}{2}S)$] is a robust prediction that does not depend on the Gaussian approximation Eq. (5). And in Appendix B we generalize Eq. (9) to higher-order correlations and show that the expressions for $P^{(2n)}$ are much more complex as soon as $n > 2$.

IV. NUMERICAL SIMULATIONS

In order to confirm these analytical predictions, we carried out numerical simulations using the method introduced in [38] and since used extensively (see, e.g., [39]). The idea of the simulations is to take as input for the signal and idler fields Gaussian white noise with intensity corresponding to half a photon per mode. This field is numerically propagated through the system, including the nonlinear crystal. The obtained fields are used to obtain, after averaging over repetitions of the simulation and appropriate subtractions, expectation values of the four-point intensity correlations

$$I(\mathbf{x}_1,\mathbf{x}_2;\mathbf{x}'_1,\mathbf{x}'_2) = \langle\Psi|n_{\mathbf{x}_1}n_{\mathbf{x}_2}n_{\mathbf{x}'_1}n_{\mathbf{x}'_2}|\Psi\rangle \tag{10}$$

where $n_x = a_x^\dagger a_x$ is the number operator at position x. We then subtract the correlations of lower order: Accidental coincidences between nontwin photons and between nontwin signal and idler pairs (two bunched photons in an image, that do not correspond to twin photons in the other image) to obtain the genuine four-point intensity correlations.

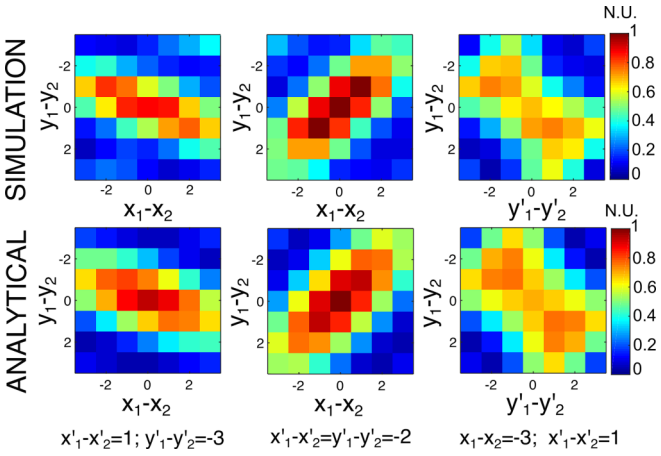

FIG. 2. Comparison of analytical predictions and numerical simulations for four-photon correlations in quantum images. To allow the comparison, the correlations of each row are normalized to unity and represented with a false color scale expressed in normalized units (N.U.). The coordinates that are not fixed in the figure are averaged out.

In Fig. 2 we compare the numerical simulations with the analytical predictions of Eq. (9). The numerical simulations were carried out for a pump beam with a waist $w_0 = 200$ μm, a crystal thickness of 50 μm, and a pump laser wavelength of 351 nm. The pixel size (used to discretize the numerical simulations) is 2.7 μm. The field of view is 256 × 256 pixels. The intensity of the pump beam is adjusted so that the intensity at the center of the signal and idler beams after propagation through the crystal is approximately 0.6 photon per pixel. The beam is then propagated 100 μm beyond the crystal in order to defocus it. The stochastic simulations were repeated 5×10^5 times in order to obtain sufficient statistics. To exhibit the oscillations of $P^{(4)}$ encoded in the variable S we fix two coordinate differences, use two other coordinate differences as plot variables, and average over the remaining four coordinates. The differences between theory and numerics correspond to a signal-to-noise ratio (SNR) of 4.9, in agreement with a model of the numerical uncertainties developed in Appendix C.

V. EXPERIMENTAL IMPLEMENTATION

Experimental parameters for an experimental implementation could be as follows: 100-fs pump pulses at 355 nm, with a waist $w_0 = 200$ μm, produce photon pairs in a β-barium borate crystal of thickness 50 μm. The noncollinear signal and idler photons pass through a 3-nm-wide notch filter to ensure that they are indistinguishable. They are imaged onto the CCD cameras with either a $2f$ or $4f$ optical system,

slightly defocused as discussed in the main text. The overall detection efficiency (the probability that a signal or idler photon is registered on the camera, taking into account all losses and detector inefficiency) can be taken to be $\eta = 0.3$. In Appendix C we estimate that 10^5 to 10^6 images need to be taken in order to reproduce experimentally images similar to those in Fig. 2. For comparison [28] used 10^7 images to analyze in detail the biphoton wave function in a quantum imaging experiment, showing that such an experiment is accessible using present technology. Two related experiments are [34], that demonstrated quantum imaging experiments with four photons but with images restricted to 4 pixels, and [40], that studied four-photon correlations but using the polarization degree of freedom.

VI. INTERPRETATION AS ENTANGLEMENT SWAPPING

The high-dimensional space in which the proposed four-photon experiment takes place makes the experiment much richer. As illustration of the features that emerge we show that a modification of the experiment allows for an interpretation as entanglement swapping [41].

Recall that initially the photon pairs shared between Alice and Bob are entangled, but there is no entanglement between Bob's photons. The joint detection of Alice's two photons projects Bob's photons into an entangled state. The intuition is that the overlap of the wave functions of Alice's two photons, followed by the detection of these two photons at specific positions, is analogous to the action of the beam splitter followed by joint detection in the teleportation experiment in [15]. Indeed, suppose we postselect that two-photon pairs are produced and that Alice's photons are detected at positions $\mathbf{x}_{A1}$ and $\mathbf{x}_{A2}$. Then it follows from Eq. (1) that Bob's two photons are projected onto the entangled state:

$$|\phi\rangle = \int d\mathbf{x}_1' d\mathbf{x}_2' [\Phi(\mathbf{x}_{A1}, \mathbf{x}_1')\Phi(\mathbf{x}_{A2}, \mathbf{x}_2') + \Phi(\mathbf{x}_{A1}, \mathbf{x}_2') \times \Phi(\mathbf{x}_{A2}, \mathbf{x}_1')] a^\dagger_{\mathbf{x}_1'} a^\dagger_{\mathbf{x}_2'} |0\rangle. \quad (11)$$

To illustrate this in more detail, suppose that $\mathbf{x}_{A1} = (+a, 0)$ and $\mathbf{x}_{A2} = (-a, 0)$, that the biphoton wave function is given by Eq. (8), and that Bob's photons are postselected to be in the vicinity of $(+l, 0)$ and $(-l, 0)$. For large enough defocusing, and small enough values of a and l, the quantum state Eq. (11) is approximately given by a momentum entangled state (see Appendix D for the derivation):

$$|\phi\rangle \approx (e^{i\varphi_1} |p'_{-+}; +l\rangle |p'_{+-}; -l\rangle + e^{i\varphi_2} |p'_{--}; +l\rangle |p'_{++}; -l\rangle) \quad (12)$$

where $\varphi_{1,2}$ are unimportant phases, and $|p'; \pm l\rangle$ are approximate momentum states located near $(\pm l, 0)$, respectively, with zero momentum in the y direction, and momentum $p'_{\pm\pm} = \pm\frac{\beta l}{2} \pm \frac{\beta a}{2}$ in the x direction.

In order to demonstrate that the resulting state indeed has the form Eq. (12), one needs to measure the first photon [located near $(+l, 0)$] in the basis spanned by $|p'_{-\pm}; l\rangle$ and the second photon [located near $(-l, 0)$] in the basis spanned by $|p'_{+\pm}; -l\rangle$. Such measurements can be realized by inserting along the paths of the photons a SLM such that around regions $(\pm l, 0)$ the SLM has phase profiles which are periodic with period $2\pi/\Delta p$, with $\Delta p = p_{\pm+} - p_{\pm-} = \beta a$, and then measuring in the far field (see Fig. 3 and Appendix E).

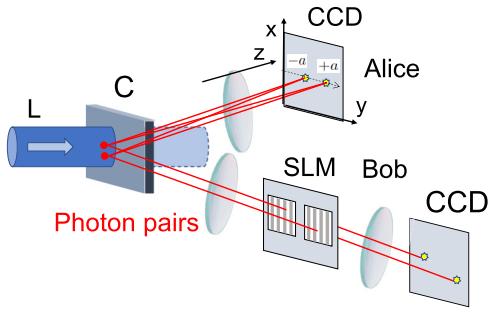

FIG. 3. Proposed setup to demonstrate entanglement swapping between quantum images (the lens indicates schematically that imaging optics is required). Alice's camera plane is defocused with respect to imaging the crystal surface (z coordinate in the image). The joint detection of Alice's photons at a specific position, say $(+a, 0)$ and $(-a, 0)$, leaves Bob's photons in an entangled state. In order to analyze the entanglement between his photons, Bob uses a SLM on which is imprinted a periodic phase profile (represented by gray lines in the figure). The SLM is positioned so as to be in the plane imaging the crystal surface. If one photon passes through one window of his SLM, and the other photon passes through the other window, then the periodic phase imprinted on the photons allows Bob to analyze the momentum entanglement between his photons. This is obtained by positioning Bob's camera in the far field (where detection events measure the transverse momentum of the photons). (The detailed procedure is described in Appendix E.)

VII. CONCLUSION

In the present paper we have shown that entangled photons of high dimension exhibit interesting multiphoton correlations, focusing on the specific case of entangled quantum images. Interesting multiphoton correlations already appear in the four-photon case. They can be exhibited by defocusing the images, which is of course easy experimentally. We provide detailed analytical predictions for the resulting four-photon interferences. These are supported by numerical simulations. We further show that this experiment can be interpreted as entanglement swapping between photons. Bob's photons are initially unentangled. But the joint detection of Alice's photons projects Bob's photons onto an entangled state.

The present paper could be extended in several directions. First of all it calls for an experimental demonstration as the multiphoton correlations described here are accessible with current experimental techniques. The main experimental difficulties are to make the different photons produced indistinguishable (except for the spatial degree of freedom) in order to allow for multiphoton interferences, and to accumulate sufficient statistics in order to see the correlations emerge from the background. As discussed above, this seems of comparable difficulty to other experiments that have been realized previously. A successful experiment of four-photon correlations would set the stage for investigating higher-order correlations (six and more photons).

Second, the proposed experiment should be compared with boson sampling experiments [17–21] whose aim is to have a

highly complex biphoton wave function in order to maximize the complexity of a classical simulations. Here we propose using a quite simple biphoton wave function, leading to simple expressions for the multiphoton correlations. However the biphoton wave function can be complexified, for instance by inserting SLMs along the optical path as proposed in [24]. Since quantum imaging experiments with hundreds to thousands of modes have been demonstrated [10,11], quantum imaging may ultimately provide a more scalable approach to boson sampling.

Third, the interpretation as entanglement swapping suggests that many multiphoton experiments such as generation of Greenberger-Horne-Zeilinger states [42], W states [43], etc., could find analog implementations using quantum imaging experiments.

Finally, the general approach proposed here is not limited to the spatial degrees of freedom. Photons entangled in other degrees of freedom, such as frequency or angular momentum, could also be used to investigate multiphoton correlations. These directions in which the present paper can be extended show that multiphoton correlation between quantum images promises to be a rich area of study, both theoretically and experimentally.

APPENDIX A: ROBUSTNESS

In this section we show that in the limit of large defocusing our results do not depend on the Gaussian approximation used in the main text. We derive a form for the biphoton wave function and for the four-photon coincidence probabilities that is valid when $z+z'$ is large.

In order to compare the results obtained in this section with the results obtained in the main text, we note that when $z+z'$ is large Eq. (8) in the main text takes the form

$$\Phi(\mathbf{x},\mathbf{x}';z,z') \approx \exp\left(-\frac{k^2}{b^2(z+z')^2}|\mathbf{x}-\mathbf{x}'|^2 + i\frac{k}{2(z+z')}|\mathbf{x}-\mathbf{x}'|^2\right).$$

In general the biphoton wave function at transverse positions $\mathbf{x}$ and $\mathbf{x}'$ on Alice's and Bob's cameras, which are positioned a distance z and z' from the nonlinear crystal, is given by

$$\Phi(\mathbf{x},\mathbf{x}';z,z') \propto \iint d\mathbf{p}d\mathbf{p}'\ \tilde{\Phi}(\mathbf{p},\mathbf{p}') \times \exp\left(-i\frac{z}{2k}|\mathbf{p}|^2 - i\frac{z'}{2k}|\mathbf{p}'|^2 + i\mathbf{p}\cdot\mathbf{x} + i\mathbf{p}'\cdot\mathbf{x}'\right) \tag{A1}$$

where $\Phi(\mathbf{p},\mathbf{p}')$ is the biphoton wave function (in momentum space) at the crystal surface, which we no longer take to be Gaussian.

We place ourselves in the translation invariant limit, so that

$$\tilde{\Phi}(\mathbf{p},\mathbf{p}') = \delta(\mathbf{p}+\mathbf{p}')\tilde{f}\left(\frac{\mathbf{p}-\mathbf{p}'}{2}\right). \tag{A2}$$

Equation (A2) therefore becomes

$$\Phi(\mathbf{x},\mathbf{x}';z,z') \propto \int d\mathbf{p}\ \tilde{f}(\mathbf{p}) \times \exp\left(-i\frac{(z+z')}{2k}|\mathbf{p}|^2 + i\mathbf{p}\cdot(\mathbf{x}-\mathbf{x}')\right). \tag{A3}$$

We suppose that the crystal is not very thick, so that at the crystal surface the photons are highly correlated in position. This implies that f (the Fourier transform of $\tilde{f}$) is strongly peaked around zero, and hence that $\tilde{f}$ is a slowly varying function. Therefore, for large enough $z+z'$, the integral in Eq. (A4) can be approximated by saddle-point integration. The saddle is at

$$\mathbf{p}^* = \frac{k(\mathbf{x}-\mathbf{x}')}{z+z'} \tag{A4}$$

and $\Phi(\mathbf{x},\mathbf{x}';z,z')$ is approximately given by

$$\Phi(\mathbf{x},\mathbf{x}';z,z') \approx \tilde{f}\left(\frac{k(\mathbf{x}-\mathbf{x}')}{z+z'}\right)\exp\left(i\frac{k}{2(z+z')}|\mathbf{x}-\mathbf{x}'|^2\right). \tag{A5}$$

This can be compared with Eq. (A1). We see that the quadratic phase of Φ is a robust prediction of the model. On the other hand the Gaussian prefactor is not.

Upon inserting Eq. (A6) into Eq. (4), one finds that the four-photon correlation probability takes the form

$$P^{(2)}(\mathbf{x}_1,\mathbf{x}_2;\mathbf{x}'_1,\mathbf{x}'_2;z,z') \propto |\tilde{f}_{11'}|^2|\tilde{f}_{22'}|^2 + |\tilde{f}_{12'}|^2|\tilde{f}_{21'}|^2 + 2|\tilde{f}_{11'}\tilde{f}_{22'}\tilde{f}_{12'}\tilde{f}_{21'}| \times \cos\left(\frac{k}{z+z'}(\mathbf{x_1}-\mathbf{x}'_1)\cdot(\mathbf{x_2}-\mathbf{x}'_2)+\varphi\right) \tag{A6}$$

where we use the notation

$$\tilde{f}_{ij'} = \tilde{f}\left(\frac{k(\mathbf{x}_i-\mathbf{x}'_j)}{z+z'}\right) \tag{A7}$$

for the slowly varying prefactors, and φ is the phase of $\tilde{f}_{11'}\tilde{f}_{22'}\tilde{f}^*_{12'}\tilde{f}^*_{21'}$.

Equation (A7) has the same structure as Eq. (9) in the main text. In particular the last term in Eq. (A7) corresponds to the oscillating term $\cos(\beta S/4)$ in Eq. (9). The argument of the harmonic function is the same $(\beta S/4)$ in both expressions, up to the phase φ.

Further note that when $\mathbf{x}_1$, $\mathbf{x}_2$, $\mathbf{x}'_1$, and $\mathbf{x}'_2$ are all close to each other, then we have approximate equality of the prefactors $\tilde{f}_{11'} = \tilde{f}_{22'} = \tilde{f}_{12'} = \tilde{f}_{21'} = \tilde{f}(\mathbf{0})$, and consequently $\varphi = 0$, and therefore Eq. (A7) further simplifies to

$$P^{(2)}(\mathbf{x}_1,\mathbf{x}_2;\mathbf{x}'_1,\mathbf{x}'_2;z,z') \propto 2|\tilde{f}(\mathbf{0})|^4\left[1+\cos\left(\frac{k}{z+z'}(\mathbf{x_1}-\mathbf{x}'_1)\cdot(\mathbf{x_2}-\mathbf{x}'_2)\right)\right]. \tag{A8}$$

Equations (A6) and (A8) show that the oscillation in the four-photon probabilities is thus a robust prediction of the proposed experiment.

APPENDIX B: HIGHER-ORDER CORRELATIONS

In this section we give expressions for higher-order correlations in quantum imaging experiments, i.e., between n photons on Alice's camera and n photons on Bob's camera. The case $n = 2$ yields Eq. (9) in the main text.

The amplitude to find n photons on Alice's camera at positions $\mathbf{x}_1, \cdots, \mathbf{x}_n$ and n photons on Bob's camera at positions $\mathbf{x'}_1, \cdots, \mathbf{x'}_n$ is given by

$$\begin{aligned}
&\langle 0|a_{\mathbf{x}_1} \cdots a_{\mathbf{x}_n} a_{\mathbf{x'}_1} \cdots a_{\mathbf{x'}_n}|\Psi\rangle \\
&\quad \propto \mathrm{Perm}(\Phi_{\mathbf{x}_1,\cdots,\mathbf{x}_n;\mathbf{x'}_1,\cdots,\mathbf{x'}_n}) \\
&\quad = \sum_\sigma \exp\left(-\frac{\alpha - i\beta}{4} \sum_{i=1}^n |x_i - x'_{\sigma(i)}|^2\right) \\
&\quad = \exp\left(-\frac{\alpha - i\beta}{4} D^{(n)}\right) \sum_\sigma \exp\left(-\frac{\alpha - i\beta}{4} S_\sigma^{(n)}\right) \qquad \text{(B1)}
\end{aligned}$$

where we have used Eq. (8) in the main text for the biphoton wave function, and where

$$D^{(n)} = \frac{1}{n} \sum_{i,j=1}^n |x_i - x'_j|^2, \qquad \text{(B2)}$$

$$\begin{aligned}
S_\sigma^{(n)} &= \sum_{i=1}^n \left(|x_i - x'_{\sigma(i)}|^2 - \frac{1}{n} \sum_{j=1}^n |x_i - x'_j|^2 \right) \\
&= 2 \sum_{i=1}^n \left(x_i \cdot x'_{\sigma(i)} - \frac{1}{n} \sum_{j=1}^n x_i \cdot x'_j \right). \qquad \text{(B3)}
\end{aligned}$$

[Note that $D^{(2)} = 2D$ where $D^{(2)}$ is defined in Eq. (B2) and D is defined in the main text below Eq. (9).]

We therefore find that

$$\begin{aligned}
P^{(n)}(\mathbf{x}_1, \cdots, \mathbf{x}_n; \mathbf{x'}_1, \cdots, \mathbf{x'}_n) &\propto \exp\left(-\frac{\alpha}{2} D^{(n)}\right) \left| \sum_\sigma \exp\left(-\frac{\alpha - i\beta}{4} S_\sigma^{(n)}\right) \right|^2 \\
&= \exp(-\frac{\alpha}{2} D^{(n)}) \left[\sum_\sigma \exp\left(-\frac{\alpha}{2} S_\sigma^{(n)}\right) + 2 \sum_{\sigma<\sigma'} \exp\left(-\frac{\alpha}{4}\left(S_\sigma^{(n)} + S_{\sigma'}^{(n)}\right)\right) \cos\left(\frac{\beta}{4}\left(S_\sigma^{(n)} - S_{\sigma'}^{(n)}\right)\right) \right] \qquad \text{(B4)}
\end{aligned}$$

[where by $\sum_{\sigma<\sigma'}$ we mean that we do a double sum over all permutations, with $\sigma \neq \sigma'$, and each pair (σ, σ') is only counted once].

Equation (B4) contains $\frac{n!(n!+1)}{2}$ terms. In the case $n = 2$ the expression simplifies because there are only two permutations, the identity I and σ_{12}, and also because we have that $S_I^{(2)} = -S_{\sigma_{12}}^{(2)}$. This yields Eq. (9) in the main text. In the case $n = 3$ there are six permutations, corresponding to 21 terms. The complexity of the multiphoton correlations thus grows rapidly as the number of photons increases.

APPENDIX C: SIGNAL-TO-NOISE RATIO

Here we estimate the SNR in the proposed experiment, and hence the number of camera frames required to reach a desired SNR. We present a qualitative estimate that shows the dependence on the main parameters. For instance our estimates are only valid for a low or moderate number of produced pairs, and we do not take into account effects due to the interference effects described in the main text (this is precisely the signal we want to measure). A more precise estimate would compute exactly all the probabilities for the signal we want to measure and all the backgrounds. This goes beyond the present paper.

1. Parameters

.For ease of reading, we list here the parameters that will be used in our analysis.

(1) $\overline{N}$ is the average number of photons produced by the pump pulse.

(2) $n_{\mathrm{Pixels}} \gg 1$ is the number of pixels over which photons can be registered. Note that this does not necessarily correspond to the number of pixels of the camera as one may bin several camera pixels together, and on the other hand part of the camera area may not be used.

(3) $0 < \eta < 1$ is the probability that a photon is detected. $(1 - \eta)$ are the losses, including all optical losses, detector efficiency, etc.)

(4) $n_{\mathrm{PixelsCond}} > 1$ is the number of pixels over which Bob's photon can be found, given that Alice detected a photon at a specific pixel.

(5) P_1 denotes the probability that a photon is registered on a pixel of Alice's camera (or a pixel of Bob's camera).

(6) P_2^{Coincid} denotes the probability that two photons from a pair are registered, one on Alice's camera and one on Bob's cameras.

(7) P_4^{Coincid} denotes the probability that four photons from two pairs are registered, two on Alice's camera and two on Bob's cameras.

(8) n^{frames} is the number of camera frames accumulated to get sufficient statistics.

(9) P_{dark} is the probability of a dark count. We will take $P_{\mathrm{dark}} = 0$ below (supposing that it is not the dominant source of noise). We indicate below how to take into account $P_{\mathrm{dark}} \neq 0$.

(10) n^{temp} is the number of temporal or spectral modes of Alice's and Bob's photons. We will initially suppose that there is a single temporal mode (i.e., that the pump pulse is sufficiently short, and subsequent spectral filtering of signal and idler sufficiently narrow, that the down-converted photons cannot be distinguished based on temporal-spectral

information). We will then show how our estimates change when there is more than one temporal mode.

2. Single pixel detection probability

The probability of having a click on a given pixel i of Alice's camera (or i' of Bob's camera) is

$$P_1(i) = P_1(i') = \eta \frac{\overline{N}}{n_{\text{Pixels}}}. \tag{C1}$$

3. Two-photon coincidence probability

If Alice registers a photon at pixel i, then the other photon of the pair can be registered over a certain zone Z_i of the Bob's camera. Let us consider the probability of a coincidence (i, i') where i' belongs to the zone Z_i:

$$\begin{aligned} P_2^{\text{Coincid}}(i, i') &= P_1(i) P^{\text{Coincid}}(i'|i) \\ &= P_1(i) \frac{\eta}{n_{\text{PixelsCond}}} \end{aligned} \tag{C2}$$

where $P^{\text{Coincid}}(i'|i)$ is the probability that Bob detects the partner photon at pixel i', given that Alice detected a photon from the same pair at pixel i.

4. Four-photon coincidence probability

What is the probability that Alice detects photons at pixels i and j and Bob detects photons at pixels i' and j'? The interesting case is when $i', j' \in Z_i$, that is, photon i' could be the partner of photon i or of j, and similarly for j'. Then there can be interferences between the different pairs. This is given by

$$P_4^{\text{Coincid}}(ij, i'j') = P_2^{\text{Coincid}}(i, i') P_2^{\text{Coincid}}(jj') \tag{C3}$$

(up to order-1 factors due to the interferences described in the main text, which is precisely what we want to measure). Thus

$$P_4^{\text{Coincid}} = \left(P_2^{\text{Coincid}}\right)^2 = \left(P_1 \frac{\eta}{n_{\text{PixelsCond}}}\right)^2. \tag{C4}$$

5. Total coincidence probabilities

The probability of a click on one pixel is

$$P(\text{click}) = P_1 + P_{\text{dark}} \tag{C5}$$

where we indicate how to take into account the dark counts. We neglect P_{dark} in what follows, but it could be easily be included in the estimates of the SNR.

The total probability of a coincidence (i, i') where i' belongs to the zone Z_i on one image is

$$P_2^{\text{CoincidTotal}}(i, i') = P_2^{\text{Coincid}}(i, i') + [P(\text{click})]^2 \tag{C6}$$

where the second term is due to accidental coincidences.

The probability of a fourfold coincidence is

$$\begin{aligned} &P_4^{\text{CoincidTotal}}(ij, i'j'|1 \text{ image}) \\ &\quad = P_4^{\text{Coincid}}(ij, i'j'|1 \text{ temp mode}) + [P(\text{click})]^4 + \dots \end{aligned} \tag{C7}$$

where the second term is due to accidental fourfold coincidences (there are other accidental kinds of fourfold coincidences, for instance when two photons belong to a pair, and the other two do not; for simplicity we do not write all these terms).

6. SNR for two-photon correlations

To measure the correlations, we need to accumulate n^{frames} camera images.

The number of single detections on pixel i is

$$N_1(i) = n^{\text{frames}} P(\text{click}) \pm \sqrt{n^{\text{frames}} P(\text{click})} \tag{C8}$$

where we add the statistical uncertainty.

The number of coincidences on pixels i and i' follows from Eq. (C6):

$$N_2^{\text{coincid}}(i, i') = n^{\text{frames}} P_2^{\text{Coincid}} + n^{\text{frames}} P(\text{click})^2. \tag{C9}$$

The signal we want to measure is

$$\text{S}_2 = n^{\text{frames}} P_2^{\text{Coincid}} \tag{C10}$$

while the noise is the statistical fluctuations of the two terms in Eq. (C9):

$$\text{N}_2 = \pm\sqrt{n^{\text{frames}} P_2^{\text{Coincid}}} + \pm\sqrt{n^{\text{frames}} P(\text{click})^2}. \tag{C11}$$

The first noise term will dominate when we have low pump power so that photon pairs are rare, while the second noise term will dominate when photon pairs are common. The two noise terms are of comparable magnitude when $P(\text{click})^2 = P_2^{\text{Coincid}}$ which corresponds to

$$\overline{N} = \frac{n_{\text{Pixels}}}{n_{\text{PixelsCond}}}. \tag{C12}$$

That is, the two noise terms are comparable when approximately one pair is produced per zone of size $n_{\text{PixelsCond}}$. Since the first noise term is the fluctuations of the signal, to improve the SNR ratio we should increase the pump power (i.e., increase $\overline{N}$) until the second noise term becomes comparable to the first. From now on we assume that this is the case, and that the first noise term is smaller than or equal to the second.

The SNR is then

$$\text{SNR}_2 = \sqrt{n^{\text{frames}}} \frac{P_2^{\text{Coincid}}}{P_1}. \tag{C13}$$

Hence the number of frames needed to exhibit two-photon coincidences is

$$\begin{aligned} n_2^{\text{frames}} &= \text{SNR}_2^2 \frac{P_1}{P_2^{\text{Coincid}}} \\ &= \text{SNR}_2^2 \frac{n_{\text{PixelsCond}}^2}{\eta^2}. \end{aligned} \tag{C14}$$

7. SNR for four-photon correlations

Similarly the number of fourfold coincidences on pixels $i, j, i',$ and j' follows from Eq. (C7):

$$\begin{aligned} N_4^{\text{Coincid}}(ij, i'j') &= n^{\text{frames}} P_4^{\text{Coincid}}(ij, i'j') \\ &\quad + n^{\text{frames}} P(\text{click})^4 + \dots. \end{aligned} \tag{C15}$$

The signal we want to measure is

$$S_4 = n^{\text{frames}} P_4^{\text{Coincid}} \tag{C16}$$

while the noise is the statistical fluctuations of the two terms in Eq. (C15):

$$N_4 = \pm\sqrt{n^{\text{frames}} P_4^{\text{Coincid}}} + \pm\sqrt{n^{\text{frames}} P(\text{click})^4}. \tag{C17}$$

One easily shows that two noise terms are comparable when Eq. (C12) is satisfied. To make the SNR ratio maximal, one should work in a regime where the pump power is large enough that the first noise term is smaller than or equal to the second.

The SNR is then

$$\begin{aligned} \text{SNR}_4 &= \sqrt{n^{\text{frames}}} \frac{P_4^{\text{Coincid}}}{P_1^2} \\ &= \sqrt{n^{\text{frames}}} \left(\frac{P_2^{\text{Coincid}}}{P_1} \right)^2 \\ &= \sqrt{n^{\text{frames}}} \frac{\eta^2}{n_{\text{PixelsCond}}^2}. \end{aligned} \tag{C18}$$

Hence the number of frames needed to exhibit four-photon coincidences is

$$\begin{aligned} n_4^{\text{frames}} &= \text{SNR}_4^2 \left(\frac{P_1}{P_2^{\text{Coincid}}} \right)^4 \\ &= \text{SNR}_4^2 \frac{n_{\text{PixelsCond}}^4}{\eta^4}. \end{aligned} \tag{C19}$$

8. Effect of distinguishable photons

If one uses a long pump pulse (or equivalently a too broad spectral filter), then photon pairs produced at different times will be distinguishable. This situation would also arise if the pump pulses were short enough, but the camera averages over several successive pump pulses. We denote n_{temp} the number of temporal modes that are averaged over in one camera frame.

Then we have that P_1, P_2^{Coincid}, and P_4^{Coincid} are all multiplied by n_{temp}.

Therefore the factor n_{temp} cancels in the SNR for photon pairs Eq. (C13). Hence one can study the photon pair correlations using a clockwise pump (which is often done experimentally).

However the factor n_{temp} does not cancel in the SNR for four-photon coincidences. Indeed only a fraction $1/n_{\text{temp}}$ fourfold coincidences will come from indistinguishable pairs while all other fourfold coincidences will come from distinguishable pairs and will contribute to background but not to the desired signal. Hence we will have

$$\text{SNR}_4 \to \frac{\text{SNR}_4}{\sqrt{n_{\text{temp}}}} \tag{C20}$$

and

$$n_4^{\text{frames}} \to n_{\text{temp}} n_4^{\text{frames}}. \tag{C21}$$

9. Estimation of the number of frames needed

We assume the following parameters:

$$\begin{aligned} \eta &= 0.3, \\ n_{\text{PixelsCond}} &= 30, \\ \text{SNR} &= 10, \\ \frac{n_{\text{Pixels}}}{n_{\text{PixelsCond}}} &= 10^3. \end{aligned} \tag{C22}$$

The last estimate expresses the fact that the total size of a camera image is much larger than the zone over which photons are correlated. Hence a single camera image contains effectively $\frac{n_{\text{Pixels}}}{n_{\text{PixelsCond}}}$ independent images, each covering a zone of size $n_{\text{PixelsCond}}$, and the number of frames that need to be taken is reduced by this factor.

Hence from Eq. (C14) we have

$$n_2^{\text{frames}} = 10^3 \tag{C23}$$

and from Eq. (C19)

$$n_4^{\text{frames}} = 10^7. \tag{C24}$$

This estimate is reduced if one wants to obtain a figure such as Fig. 2 in the main text, as in this figure $K \approx 50$ fourfold correlations are averaged to obtain each pixel in the figure. To obtain the same SNR, the number of frames required is reduced by a factor K (see discussion in the next subsection). We thus reach an estimate between 10^5 and 10^6 frames to reproduce experimentally a figure such as Fig. 2.

10. Comparison between analytics and simulations in Fig. 2

In the simulation, we perform for each pixel of Fig. 2 an average of $K = 49$ values of fourfold correlations between Alice's pixels of coordinates $\mathbf{x_1}$ and $\mathbf{x_2}$ and Bob's pixels of coordinates $\mathbf{x_1'}$ and $\mathbf{x_2'}$. The averaged values correspond to a unique value of $\mathbf{x_1} - \mathbf{x_2}, \mathbf{x_1'} - \mathbf{x_2'}$. This averaging multiplies the SNR by $\sqrt{S}$, giving, in the conditions of the simulation corresponding to $n_{\text{temp}} = 1$, $\eta = 1$, an expected SNR of

$$\text{SNR} = \frac{\sqrt{S}\sqrt{n_{\text{frames}}}}{n_{\text{PixelsCond}}^2}. \tag{C25}$$

With $n_{\text{frames}} = 5 \times 10^5$, $n_{\text{PixelsCond}} = 32$, we obtain with Eq. (C25) an SNR of 4.8. This value of $n_{\text{PixelsCond}}$ seems reasonable because of the decreasing of the correlations close to the edges of the subfigures in Fig. 2.

We can compare this with the SNR estimated from the images by comparing the analytical and the simulated values in Fig. 2. This gives an estimated SNR of

$$\text{SNR}_{\text{est}} = \frac{\overline{\text{Analytic}}}{\sqrt{\overline{(\text{Analytic} - \text{simulated})^2}}} = 4.9. \tag{C26}$$

There is thus a good agreement between the two estimates.

APPENDIX D: ENTANGLEMENT SWAPPING

We give here details about the interpretation in terms of entanglement swapping.

We suppose that the biphoton wave function is given by Eq. (8) and that Alice detects her photons at positions $\mathbf{x}_{A1} = (+a, 0)$ and $\mathbf{x}_{A2} = (-a, 0)$. We denote the transverse coordinates on Bob's detection plane by $\mathbf{x}'_1 = (x'_1, y'_1)$ and $\mathbf{x}'_2 = (x'_2, y'_2)$. Then the wave function of Bob's two photons takes the form [insert Eq. (8) into Eq. (11)]

$$\begin{aligned}|\phi\rangle &= \exp\left(-\frac{\alpha - i\beta}{4}\left[(a - x'_1)^2 + {y'_1}^2 + (a + x'_2)^2 + {y'_2}^2\right]\right) + \exp\left(-\frac{\alpha - i\beta}{4}\left[(a + x'_1)^2 + {y'_1}^2 + (a - x'_2)^2 + {y'_2}^2\right]\right)\\ &= \exp\left(-\frac{\alpha - i\beta}{4}\left({y'_1}^2 + {y'_2}^2\right)\right)\exp\left(-\frac{\alpha - i\beta}{4}\left(2a^2 + {x'_1}^2 + {x'_2}^2\right)\right)\\ &\quad\times\left[\exp\left(-\frac{\alpha - i\beta}{2}a(x'_2 - x'_1)\right) + \exp\left(-\frac{\alpha - i\beta}{2}a(x'_1 - x'_2)\right)\right].\end{aligned} \tag{D1}$$

We suppose that $\mathbf{x}'_1 = (x'_1, y'_1)$ and $\mathbf{x}'_2 = (x'_2, y'_2)$ are located in the vicinity of $(l, 0)$ and $(-l, 0)$. We then write

$$x'_1 = l + \delta'_1, \quad x'_2 = -l + \delta'_2. \tag{D2}$$

We bound the region in which Bob's particles can be located by

$$\begin{aligned}-\delta \leqslant \delta'_1, \delta'_2 \leqslant +\delta,\\ -y \leqslant y'_1, y'_2 \leqslant +y\end{aligned} \tag{D3}$$

with

$$\delta \ll l. \tag{D4}$$

In order to simplify Eq. (D1) we make the following assumptions:

$\beta \gg \alpha$ (large defocusing, i.e., $Z \gg 1$),

$(\alpha, \beta) \times y \ll 1$ (neglect y dependence),

$(a^2, al, l^2) \times \alpha \ll 1$ (neglect all terms that depend on α),

$\delta^2\beta \ll 1$ (neglect second-order terms in δ'_1, δ'_2),

$(a^2, al, l^2) \times \beta \gg 1$ (keep phases proportional to β).

With these assumptions Eq. (D1) takes the form

$$\begin{aligned}\phi \simeq \exp\left(i\frac{\beta}{2}(a^2 + l^2)\right)&\times\left[\exp\left(i\frac{\beta}{2}[-2al + (l - a)\delta'_1 - (l - a)\delta'_2]\right)\right.\\ &\left.+\exp\left(i\frac{\beta}{2}[+2al + (l + a)\delta'_1 - (l + a)\delta'_2]\right)\right]\end{aligned} \tag{D5}$$

which we can rewrite in terms of momentum states as

$$\begin{aligned}|\phi\rangle \simeq \exp\left(i\frac{\beta}{2}(a^2 + l^2)\right)&\left(\exp(-i\beta al)\left|p'_1 = -\frac{\beta l}{2} + \frac{\beta a}{2}; +l\right\rangle\left|p'_2 = +\frac{\beta l}{2} - \frac{\beta a}{2}; -l\right\rangle + \exp(+i\beta al)\left|p'_1\right.\right.\\ &\left.\left. = -\frac{\beta l}{2} - \frac{\beta a}{2}; +l\right\rangle\left|p'_2 = +\frac{\beta l}{2} + \frac{\beta a}{2}; -l\right\rangle\right).\end{aligned} \tag{D6}$$

This is the expression given in the main text in Eq. (12).

APPENDIX E: DEMONSTRATING ENTANGLEMENT SWAPPING

In the main text we sketched how to demonstrate experimentally that state Eq. (D6) is entangled by inserting a SLM in the beam of Bob's photons (see Fig. 3 in the main text). We present here the argument in more detail.

The state Eq. (D6) is a two-qubit state, which we can write in abstract notation as

$$|\phi\rangle = a|0\rangle_B|0\rangle_{B'} + b|1\rangle_B|1\rangle_{B'} \tag{E1}$$

where

$$\begin{aligned}a &= \exp(-i\beta al),\\ b &= \exp(+i\beta al),\\ |0\rangle_B &= \left|p'_1 = -\frac{\beta l}{2} + \frac{\beta a}{2}; +l\right\rangle,\\ |1\rangle_B &= \left|p'_1 = -\frac{\beta l}{2} - \frac{\beta a}{2}; +l\right\rangle,\\ |0\rangle_{B'} &= \left|p'_2 = +\frac{\beta l}{2} - \frac{\beta a}{2}; -l\right\rangle,\\ |1\rangle_{B'} &= \left|p'_2 = +\frac{\beta l}{2} + \frac{\beta a}{2}; -l\right\rangle,\end{aligned} \tag{E2}$$

and where the subscripts B and B' denote the photons that are located near $+l$ and $-l$, respectively.

Measuring in the $\{|0\rangle_B, |1\rangle_B\}$ and $\{|0\rangle_{B'}, |1\rangle_{B'}\}$ bases is straightforward. First insert a mirror to separate spatially the B states from the B' states (recall that these states are localized in momentum and in space). Then put the CCD camera in the far field.

But measuring only in the computational basis (the basis $\{|0\rangle, |1\rangle\}$) is not enough to demonstrate entanglement. For this we need additional measurements. We show how to do so using a SLM.

Suppose that we put on the SLM a periodic phase profile $\varphi(x) = \epsilon \cos(kx + \theta)$. Then a wave function $\psi(x)$ becomes

$$\psi(x) \to \psi(x) e^{i\varphi(x)}. \tag{E3}$$

We can expand the phase in Fourier series as

$$\begin{aligned} e^{i\epsilon \cos(kx+\theta)} &= \sum_n a_n(\epsilon) e^{in(kx+\theta)} \\ &\approx 1 + i\frac{\epsilon}{2} e^{i(kx+\theta)} + i\frac{\epsilon}{2} e^{-i(kx+\theta)} + O(\epsilon^2) \end{aligned} \tag{E4}$$

where the exact coefficients $a_n(\epsilon) = i^n J_n(\epsilon)$ follow from the Jacobi-Anger expansion (with J_n the Bessel function of the first kind). In the second line we give the expression for small ϵ which we use below as it is conceptually simpler, and sufficient to demonstrate the principle.

From Eq. (E4) it follows that acting on a momentum state $|p\rangle$, the SLM carries out the transformation

$$|p\rangle \to |p\rangle + i\frac{\epsilon e^{i\theta}}{2}|p-k\rangle + i\frac{\epsilon e^{-i\theta}}{2}|p+k\rangle. \tag{E5}$$

Acting on the superposition of two momentum states $|\psi\rangle = \alpha|p\rangle + \beta|p+k\rangle$ (where we suppose that the momenta differ by exactly the wave number k of the SLM phase), we therefore have

$$\begin{aligned} |\psi\rangle = \alpha|p\rangle + \beta|p+k\rangle \to i\frac{\epsilon e^{i\theta}}{2}\alpha|p-k\rangle + \left(\alpha + i\frac{\epsilon e^{i\theta}}{2}\beta\right)|p\rangle \\ + \left(\beta + i\frac{\epsilon e^{-i\theta}}{2}\alpha\right)|p+k\rangle + i\frac{\epsilon e^{-i\theta}}{2}\beta|p+2k\rangle. \end{aligned} \tag{E6}$$

By measuring in the far field, the probability of finding the photon in spots corresponding to momenta p and $p+k$ will be equal to the norm square of the coefficients of the second and third line in Eq. (E6). These probabilities are proportional to

$$\begin{aligned} &\left|\left(\langle p| - i\frac{\epsilon e^{-i\theta}}{2}\langle p+k|\right)|\psi\rangle\right|^2, \\ &\left|\left(-i\frac{\epsilon e^{+i\theta}}{2}\langle p| + \langle p+k|\right)|\psi\rangle\right|^2, \end{aligned} \tag{E7}$$

respectively.

Therefore by both measuring in the original $\{|p\rangle, |p+k\rangle\}$ basis and carrying out the above measurement for different values of θ (for fixed ϵ) one easily obtains tomographically complete information on the state.

Note that using the Jacobi-Anger expansion mentioned in Eq. (E4), one can carry out the above analysis for a finite value of ϵ. One finds for instance that the probabilities for the far-field probabilities at momenta p and $p+k$ are given by

$$\begin{aligned} &|(a_0^*\langle p| + a_1^* e^{-i\theta}\langle p+k|)|\psi\rangle|^2, \\ &|(a_{-1}^* e^{+i\theta}\langle p| + a_0^*\langle p+k|)|\psi\rangle|^2 \end{aligned} \tag{E8}$$

instead of the approximate expression Eq. (E7).

Going back to the problem Eqs. (E1) and (E2), we see that choosing $k = \beta a$ for the wave number of the phase on the SLM will allow one to do a tomographically complete set of measurements on the state Eq. (E1).

[1] S. J. Freedman and J. F. Clauser, Experimental Test of Local Hidden-Variable Theories, Phys. Rev. Lett. **28**, 938 (1972).

[2] A. Aspect and J. Dalibard, Experimental Test of Bell's Inequalities Using Time-Varying Analyzers, Phys. Rev. Lett. **49**, 1804 (1982).

[3] A. C. Dada, J. Leach, G. S. Buller, M. J. Padgett, and E. Andersson, Experimental high-dimensional two-photon entanglement and violations of generalized Bell inequalities, Nat. Phys. **7**, 677 (2011).

[4] M. Krenn, M. Huber, R. Fickler, R. Lapkiewicz, S. Ramelow, and A. Zeilinger, Generation and confirmation of a (100 × 100)-dimensional entangled quantum system, Proc. Natl. Acad. Sci. USA **111**, 6243 (2014).

[5] L. Olislager, J. Cussey, A.-T. Nguyen, P. Emplit, S. Massar, J.-M. Merolla, and K. P. Huy, Frequency-bin entangled photons, Phys. Rev. A **82**, 013804 (2010).

[6] Z. Xie, T. Zhong, S. Shrestha, X. Xinan *et al.*, Harnessing high-dimensional hyperentanglement through a biphoton frequency comb, Nat. Photonics **9**, 536 (2015).

[7] P. Imany, J. A. Jaramillo-Villegas, O. D. Odele, K. Han *et al.*, 50-GHz-spaced comb of high-dimensional frequency-bin entangled photons from an on-chip silicon nitride microresonator, Opt. Express **26**, 1825 (2018).

[8] K. C. Chang, X. Cheng, M. C. Sarihan, A. K. Vinod *et al.*, 648 Hilbert-space dimensionality in a biphoton frequency comb: Entanglement of formation and Schmidt mode decomposition, npj Quantum Inf. **7**, 48 (2021).

[9] J. C. Howell, R. S. Bennink, S. J. Bentley, and R. Boyd, Realization of the Einstein-Podolsky-Rosen Paradox Using Momentum- and Position-Entangled Photons from Spontaneous Parametric Down Conversion, Phys. Rev. Lett. **92**, 210403 (2004).

[10] M. P. Edgar, D. S. Tasca, F. Izdebki, R. E. Warburton *et al.*, Imaging high-dimensional spatial entanglement with a camera, Nat. Commun. **3**, 984 (2012).

[11] P. A. Moreau, F. Devaux, and E. Lantz, Einstein-Podolsky-Rosen Paradox in Twin Images, Phys. Rev. Lett. **113**, 160401 (2014).

[12] F. Devaux, A. Mosset, F. Bassignot, and E. Lantz, Quantum holography with biphotons of high Schmidt number, Phys. Rev. A **99**, 033854 (2019).

[13] J. Wang, S. Paesani, Y. Ding, R. Santagati *et al.*, Multidimensional quantum entanglement with large-scale integrated optics, Science **360**, 285 (2018).

[14] J. T. Barreiro, N. K. Langford, N. A. Peters, and P. G. Kwiat, Generation of Hyperentangled Photon Pairs, Phys. Rev. Lett. **95**, 260501 (2005).

[15] D. Bouwmeester, J.-W. Pan, K. Mattle, M. Eibl, H. Weinfurter, and A. Zeilinger, Experimental quantum teleportation, Nature (London) **390**, 575 (1997)

[16] S. Aaronson and A. Arkhipov, The computational complexity of linear optics, in *Proceedings of the Forty-Third Annual ACM Symposium on Theory of Computing* (Association for Computing Machinery, New York, 2011), p. 333.

[17] M. A. Broome, A. Fedrizzi, S. Rahimi-Keshari, J. Dove, S. Aaronson, T. C. Ralph and A. G. White, Photonic boson sampling in a tunable circuit, Science **339**, 794 (2013).

[18] J. B. Spring, B. J. Metcalf, P. C. Humphreys, W. S. Kolthammer *et al.*, Boson sampling on a photonic chip, Science **339**, 798 (2013).

[19] M. Tillmann, B. Dakić, R. Heilmann, S. Nolte, A. Szameit, and P. Walther, Experimental boson sampling, Nat. Photonics **7**, 540 (2013)

[20] S. Paesani, Y. Ding, R. Santagati, L. Chakhmakhchyan *et al.*, Generation and sampling of quantum states of light in a silicon chip, Nat. Phys. **15**, 925 (2019).

[21] H. S. Zhong, H. Wang, Y.-H. Deng, M.-C. Chen *et al.*, Quantum computational advantage using photons, Science **370**, 1460 (2020).

[22] L. Chakhmakhchyan and N. J. Cerf, Boson sampling with Gaussian measurements, Phys. Rev. A **96**, 032326 (2017)

[23] D. Grier, D. J. Brod, J. M. Arrazola, M. B. A. Alonso, and N. Quesada, The complexity of bipartite Gaussian boson sampling, Quantum **6**, 863 (2022).

[24] R. van der Meer, S. Huber, P. W. H. Pinkse, R. García-Patrón, and J. J. Renema, Boson sampling in low-depth optical systems, arXiv:2110.05099 (2021).

[25] M. I. Kolobov and I. V. Sokolov, Spatial behavior of squeezed states of light and quantum noise in optical images, Zh. Eksp. Teor. Fiz. **96**, 1945 (1989) [Sov. Phys. JETP **69**, 1097 (1989)]; Squeezed states of light and noise-free optical images, Phys. Lett. A **140**, 101 (1989).

[26] P.-A. Moreau, J. Mougin-Sisini, F. Devaux, and E. Lantz, Realization of the purely spatial Einstein-Podolsky-Rosen paradox in full-field images of spontaneous parametric down-conversion, Phys. Rev. A **86**, 010101(R) (2012).

[27] P. A. Morris, R. S. Aspden, J. E. C. Bell, R. W. Boyd, and M. J. Padgett, Imaging with a small number of photons, Nat. Commun. **6**, 5913 (2015).

[28] H. Defienne, M. Reichert, and J. W. Fleischer, Adaptive Quantum Optics with Spatially Entangled Photon Pairs, Phys. Rev. Lett. **121**, 233601 (2018).

[29] G. Brida, M. Genovese, and I. R. Berchera, Experimental realization of sub-shot-noise quantum imaging, Nat. Photonics **4**, 227 (2010).

[30] E. Toninelli, M. P. Edgar, P.-A. Moreau, G. M. Gibson, G. D. Hammond, and M. J. Padgett, Sub-shot-noise shadow sensing with quantum correlations, Opt. Express **25**, 21826 (2017).

[31] G. B. Lemos, V. Borish, G. D. Cole, S. Ramelow, R. Lapkiewicz, and A. Zeilinger, Quantum imaging with undetected photons, Nature (London) **512**, 409 (2014).

[32] P. A. Moreau, E. Toninelli, T. Gregory, and M. J. Padgett, Imaging with quantum states of light, Nat. Rev. Phys. **1**, 367 (2019).

[33] G. Soro, E. Lantz, A. Mosset, and F. Devaux, Quantum spatial correlations imaging through thick scattering media: Experiments and comparison with simulations of the biphoton wave function, J. Opt. **23**, 025201 (2021).

[34] N. Bornman, M. Agnew, F. Zhu, A. Vallés, A. Forbes, and J. Leach, Ghost imaging using entanglement-swapped photons, npj Quantum Inf. **5**, 63 (2019).

[35] C. K. Law and J. H. Eberly, Analysis and Interpretation of High Transverse Entanglement in Optical Parametric Down Conversion, Phys. Rev. Lett. **92**, 127903 (2004).

[36] M. V. Fedorov, M. A. Efremov, P. A. Volkov, E. V. Moreva, S. S. Straupe, and S. P. Kulik, Anisotropically and High Entanglement of Biphoton States Generated in Spontaneous Parametric Down-Conversion, Phys. Rev. Lett. **99**, 063901 (2007).

[37] K. W. Chan, J. P. Torres, and J. H. Eberly, Transverse entanglement migration in Hilbert space, Phys. Rev. A **75**, 050101(R) (2007).

[38] E. Brambilla, A. Gatti, M. Bache, and L. A. Lugiato, Simultaneous near-field and far-field spatial quantum correlations in the high-gain regime of parametric down-conversion, Phys. Rev. A **69**, 023802 (2004).

[39] E. Lantz, M. Mabed, and F. Devaux, Violation of Bell inequalities by stochastic simulations of Gaussian States based on their positive Wigner representation, Phys. Scr. **96**, 045103 (2021).

[40] M. Eibl, S. Gaertner, M. Bourennane, C. Kurtsiefer, M. Zukowski, and H. Weinfurter, Experimental Observation of Four-Photon Entanglement from Parametric Down-Conversion, Phys. Rev. Lett. **90**, 200403 (2003).

[41] C. H. Bennett, G. Brassard, C. Crépeau, R. Jozsa, A. Peres, and W. K. Wootters, Teleporting an Unknown Quantum State Via Dual Classical and Einstein-Podolsky-Rosen Channels, Phys. Rev. Lett. **70**, 1895 (1993).

[42] D. Bouwmeester, J. W. Pan, M. Daniell, H. Weinfurter, and A. Zeilinger, Observation of Three-Photon Greenberger-Horne-Zeilinger Entanglement, Phys. Rev. Lett. **82**, 1345 (1999).

[43] M. Eibl, N. Kiesel, M. Bourennane, C. Kurtsiefer, and H. Weinfurter, Experimental Realization of a Three-Qubit Entangled W State, Phys. Rev. Lett. **92**, 077901 (2004).